



Picosecond laser-ablated metal nanostructures and nanoparticles for SERS-based sensing applications

Jagannath Rathod, M S S Bharati, Chandu Byram, and Venugopal Rao Soma*

Advanced Centre of Research in High Energy Materials (ACRHEM),

University of Hyderabad, Hyderabad- 500 046, Telangana, India

We present results from our studies on the fabrication of gold (Au) nanostructures (NSs) using picosecond (ps) laser ablation in ambient air, as well as the fabrication of silver (Ag) nanoparticles (NPs) in various liquids, such as distilled water, NaOH and KOH. The synthesized Au NSs and Ag NPs are utilized as surface-enhanced Raman scattering (SERS) substrates. Au NSs sensitivity was further improved with the deposition of chemically synthesized Au nanostars. The shape and size of obtained Ag NPs and Au nanostars were investigated using transmission electron microscopy (TEM). The morphology of the laser-patterned areas on the Au surface was studied by field emission scanning electron microscope (FESEM) measurements. The Au nanostars decorated on laser-patterned Au SERS substrate exhibited superior reproducibility of the Raman signals ($< 10\%$ RSD) and better SERS enhancement factors ($\sim 10^5$) for thiram (a commonly used fungicide molecule in a variety of crops) in comparison with the laser-patterned Au (without Au nanostars) as well as Au nanostars decorated flat Au substrates. The stability of Ag NPs was studied by UV-visible absorption spectroscopic technique. Ag NPs synthesized in NaOH and KOH liquid environment are stable for 30 days compared with Ag NPs dispersed in distilled water. © Anita Publications. All rights reserved.

Keywords: laser ablation, metal nanoparticles, SERS, thiram, methylene blue, alkali metal hydroxide.

1 Introduction

Metal (Ag/Au) nanomaterials are the most studied nano-technological tools for the past two decades in various fields such as surface-enhanced Raman scattering (SERS), catalysis, bio-sensing, and bio-imaging due to their easy synthesis methods, chemical stability, bio-compatibility, and outstanding optical properties [1,2]. Especially the localized surface plasmonic property of metal nanomaterials can be tuned from the visible to near-infrared spectral region depending on their sizes and shapes [3]. In recent years, star-shaped NPs have gained tremendous interest in the SERS application because of the induced high electric fields at their sharp tips, unlike in their spherical and nanorod counterparts) [4,5]. The synthesis of Au nanoparticles in different shapes and sizes, along with greater yield, was achieved by chemical routes [6,7]. Various procedures have been reported for synthesizing Au nanostars (seedless or seed-mediated techniques, etc.) [5,8,9]. Zhu *et al* [8] have reported nanostars on apple peels with the lowest-limit detection of thiram at a concentration of 1×10^{-10} M. Recently, we have reported the fabrication of Au nanoparticles and nanostars and investigated their SERS performance. We found a higher SERS enhancement for Au nanostars than the spherical Au nanoparticles decorated on Si/filter paper-based substrates [9]. Ultrafast laser ablation is one of the best methods to synthesize various nanomaterials without any surfactants [10,11]. The nanomaterial properties depend on the

*Based on the lecture delivered at ICOPVS2022, Dec 13-17, 2022,
UGC-DAE Consortium For Scientific Research, Indore, India.*

Corresponding author

e mail: soma_venu@uohyd.ac.in (Venugopal Rao Soma)

laser parameters, focusing conditions, material parameters, and also on the surrounding medium. [12-14] The present study reports the synthesis of Au NSs in air and Ag NPs in distilled water (DIW), NaOH, and KOH. Improved sensitivity in detecting analytes was achieved by depositing Au nanostars onto the Au substrates that were ablated using a picosecond (ps) laser, resulting in significant enhancements in the SERS signals. Laser ablation in alkali metal hydroxides will improve the stability of Ag NPs compared to DIW. These Au nanostars-based SERS substrates were investigated using the thiram molecule, a pesticide primarily utilized in food industries and also using a biomolecule cytosine, which is a part of nucleotide. The alliance of ps laser-processed Au NSs and Au nanostars delivered a detectable way to achieve more significant number of hotspots. This approach could lead to the achievement of higher detection limits along with superior reproducibility over large areas.

2 Experimental section

2.1 Materials

Silver (Ag) and gold (Au) samples with 99% purity having a thickness of 0.1 mm were used as targets in ps laser ablation, chloroauric acid ($\text{HAuCl}_4 \cdot 3\text{H}_2\text{O}$), sodium hydroxide (NaOH), sodium iodide (NaI), ethanol, dimethylformamide (DMF), poly(N-vinyl-2-pyrrolidone) (PVP-40000 MW), and analyte molecules such as thiram ($\text{C}_6\text{H}_{12}\text{N}_2\text{S}_4$), Nile blue ($\text{C}_2\text{OH}_2\text{OCIN}_3\text{O}$), cytosine ($\text{C}_4\text{H}_5\text{N}_3\text{O}$) were purchased from M/s Sigma-Aldrich. All glassware were properly cleaned before conducting the experiments.

2.2 Laser ablation in air

Gold (Au) nanostructures (NSs) were achieved through ps laser ablation of Au target in the air using an axicon lens (base angle- 10°). Laser ablation experiments were conducted using an Nd: YAG laser that delivered ~ 30 ps pulses at a repetition rate of 10 Hz and a wavelength of 1064 nm. The ps laser beam having pulse energy ~ 10 mJ, was focused normally on the Au target using an axicon lens. The sample was mounted on a motorized X-Y stage (Newport). During the experiment, the sample was scanned at a speed of 2.5 mm/s along both the X and Y directions. The laser-patterned area on the sample surface was typically 25 mm^2 .

2.3 Laser ablation in liquid

Silver (Ag) nanoparticles (NPs) were synthesized using the technique of ps laser ablation of an Ag target in various liquids [deionized water (DIW), sodium hydroxide (NaOH), and potassium hydroxide (KOH)]. The Ag target was ablated with a fixed pulse energy of ~ 20 mJ and was raster-scanned at a speed of 1 mm/s along the X and Y directions with $50 \mu\text{m}$ spacing along Y-direction. The complete experimental details are given in previous work [15].

2.4 Measurements

The optical properties of colloidal nanoparticles were studied by using a UV-visible absorption spectrometer (JASCO V-670) in the wavelength range of 400–900 nm. The size and shape of NPs were confirmed by transmission electron microscopy (TEM, FE-Technai G2system operated at an accelerating voltage of 300 kV). The surface topography of laser-processed regions of Au substrate was investigated by field emission scanning electron microscopy (FESEM, Carl ZEISS). SERS measurements were conducted using a portable Raman spectrometer (M/s B&W Tek, USA) with a continuous laser source operating at a wavelength of 785 nm. We used an input laser energy of 60 mW and 5 seconds as the integration time. In the case of NSs' SERS measurements, $10 \mu\text{L}$ of Au nanostars solution was dropped on the laser-processed Au substrate (surface area of 5 mm^2) and dried. Further, the analyte ($5 \mu\text{L}$) was dropped on an earlier prepared substrate, followed by recording the SERS measurements. In the case of Ag NPs SERS measurements, the $10 \mu\text{L}$ of NPs are drop-casted on the cleaned Si and allowed to dry. Then, $5 \mu\text{L}$ of the desired analyte molecule was added, and SERS measurements were made using portable Raman spectrometer.

3 Results and Discussion

The UV-visible absorption spectra of ps laser ablated Ag and chemically synthesized Au colloidal nanoparticles are shown in Fig 1(a-d). Figure 1(a-c) represents the absorption spectra of Ag nanoparticles in (a) DIW, (b) NaOH, and (c) KOH, respectively. The NPs exhibited an optical absorption peak near 428 nm, 409 nm, and 408 nm, respectively, which is in good agreement with the reported literature [5]. In the case of Ag NPs in DIW, a broader absorption spectrum was noticed compared to alkali metal hydroxide, possibly due to the ablation medium's ionic (Na^+ and K^+) species and the variation in the size distribution [16]. In the case of Au nanostars, the peak in the visible region (582 nm) corresponds to the core, and in the NIR region (763 nm) is owing to the sharp tips of Au nanostars, Fig 1(d) [17,18].

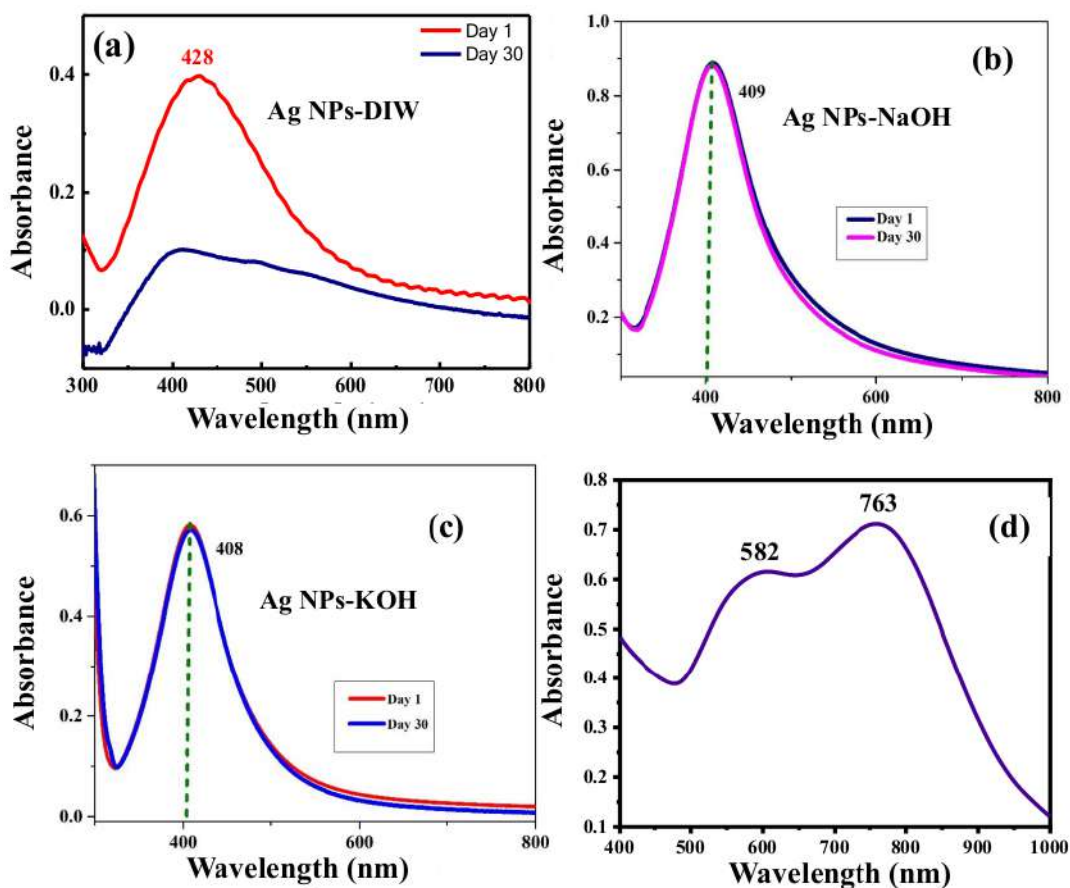


Fig 1. UV-absorption spectra of ps laser ablated Ag NPs (a) DIW (b) NaOH (c) KOH (d) chemically synthesized Au nanostars. In (a) and (c) red color curve represents the data obtained on day 1 and blue color curve represents the data obtained on day 30. In (b) blue color curve represents day 1 data while purple color curve represents day 30 data.

Figure 2 depicts the TEM images of laser-ablated Ag nanoparticles and chemically synthesized Au nanostars. The Ag NPs synthesized by picosecond laser ablation were found to be spherical in all three liquids (DIW, NaOH, and KOH). However, the size distribution of Ag NPs in DIW was found to be significantly broader than that in NaOH and KOH. Figure 2(d) represents the TEM image of Au nanostars; wherein NPs with more than 4 tips are presented.

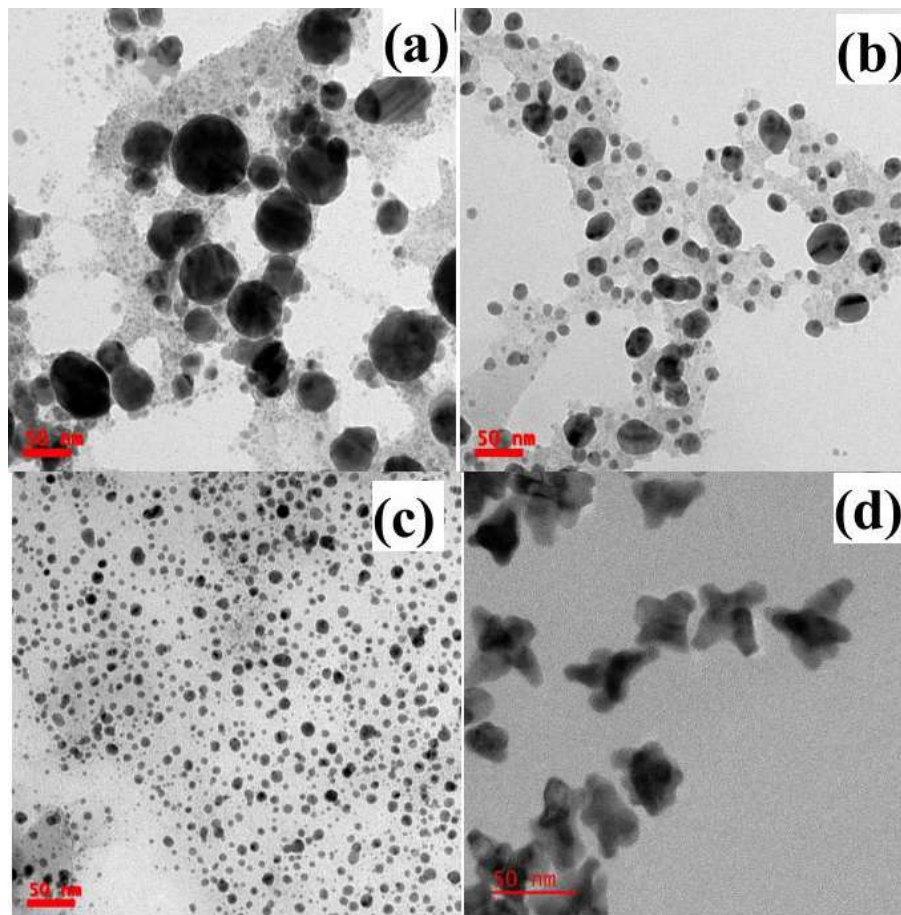


Fig 2. TEM images of ps laser ablated Ag NPs (a) DIW (b) NaOH (c) KOH (d) chemically synthesized Au nanostars (all images are shown in 50 nm scale bar).

The lower and higher magnification FESEM images of laser-processed Au nanostructures (NSs) are depicted in Fig 3(a) and 3(b), respectively. From Fig 3(a) and 3(b), it is evident that laser-processed regions of the Au NSs possessed both nano-protrusions and nanoholes. The FESEM images of Au nanostars embedded on the plain as well as laser-processed Au NSs are depicted in Figs 4(a) and 4(b), respectively. FESEM images revealed that the Au nanostars were decorated randomly throughout the area on plain and laser-processed Au substrate. The ablated metallic surface is made up of many small features, including sharp-tipped nanostars. These features create hotspots where the electric field is strongly enhanced. The enhanced electric field leads to a greater enhancement of the Raman signal. In the case of plain metallic surface the dispersed nanostars provide the hotspots.

SERS measurements

The SERS studies were performed on laser-ablated Ag NPs in different liquids (NaOH and KOH). Figure 5 represents the SERS spectra of methylene blue (MB)-5nM using Ag NPs ablated in NaOH and KOH on bare Si. The vibrational modes of MB were identified at 448, 889, 1394, and 1618 cm^{-1} and are assigned following the literature [19]. The SERS intensities from Ag NPs in NaOH were higher compared to the Ag NPs in KOH, and the reasons have to be further investigated.

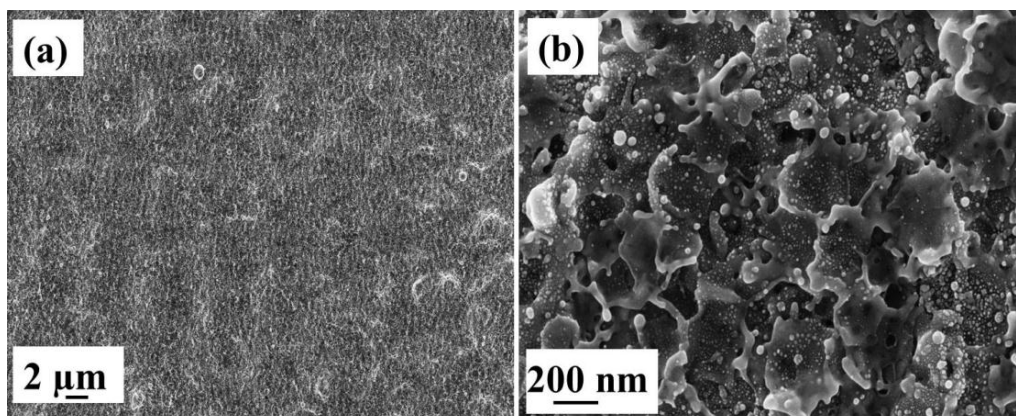


Fig 3. Lower and higher magnification FESEM images of laser-processed Au nanostructures.

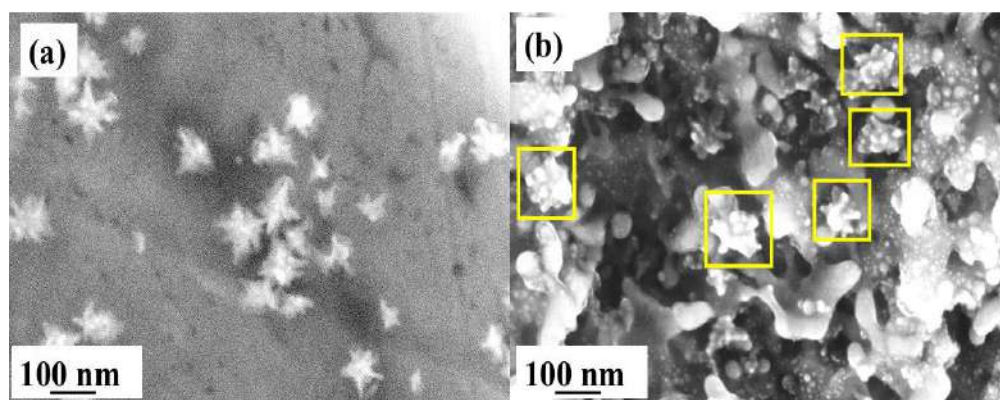


Fig 4. FESEM images of Au nanostars decorated on (a) plain (Au), (b) ps laser-processed Au NSs with 100 nm magnification bar.

Further, the SERS studies were performed for laser-processed Au and for nanostars embedded in plain Au and laser-processed Au substrates. Figure 6 (a) shows the SERS spectra of thiram ($5 \mu\text{M}$) obtained from (i) laser-processed Au (ii) nanostars embedded plain Au, (iii) laser-processed Au decorated with Au NS. The assessed intensities of the prominent mode at 1375 cm^{-1} from each substrate are shown in Fig 6(b), and it is evident that the nanostars embedded laser-processed Au exhibited higher SERS sensing than the other substrates. The probable reason for achieving higher enhancements could be due to the accumulated nanostars in the gaps of laser-processed areas, which led to the generation of a greater number of hotspots. Au nanostars embedded laser-processed Au was further utilized for detecting other analytes due to their higher SERS sensitivity.

The SERS spectra of thiram were recorded at various concentrations (ranging from $50 \mu\text{M}$ to 5 nM) on a laser-processed Au substrate decorated with chemically synthesized Au nanostars, as shown in Fig 7(a). The intensity of 1375 cm^{-1} Raman mode versus varying concentrations is shown as a log plot in Fig 7(b). The obtained R^2 value, in this case, was ~ 0.96 , Fig 7(b). The reproducibility of the SERS spectra of thiram ($50 \mu\text{M}$) recorded at 15 random positions is shown in Fig 7(c) as a 3D waterfall curve. The calculated relative standard deviation (RSD) values for 560 cm^{-1} , 1138 cm^{-1} , and 1375 cm^{-1} are shown in Fig 7(d). The observed RSD ($< 10\%$) values revealed that the substrates had an acceptable reproducibility over 25 mm^2 , as shown in Fig 7(d).

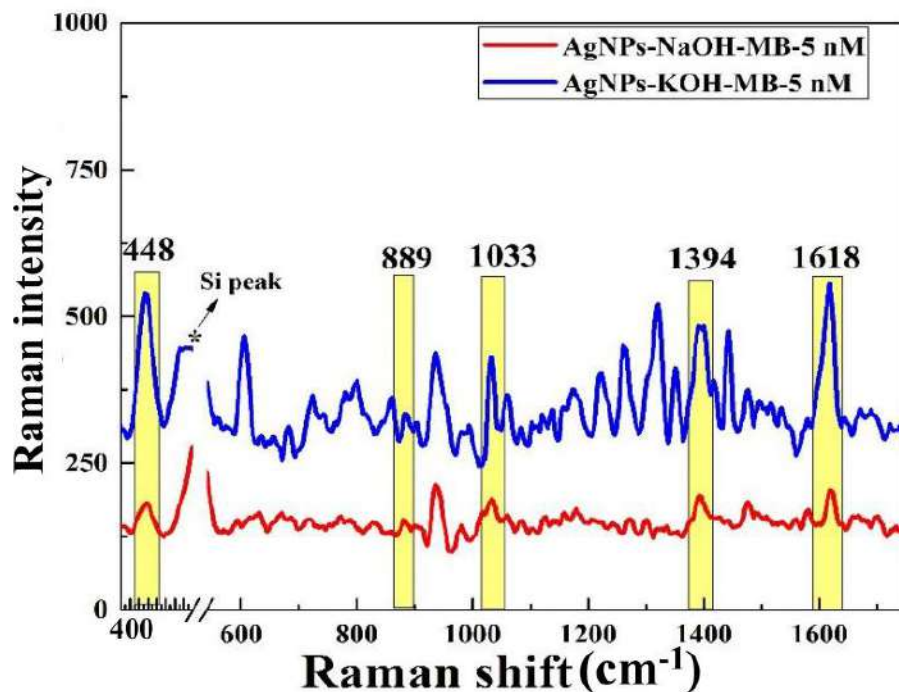


Fig 5. SERS spectra of MB-5nM using ps laser ablated Ag NPs in NaOH and KOH.

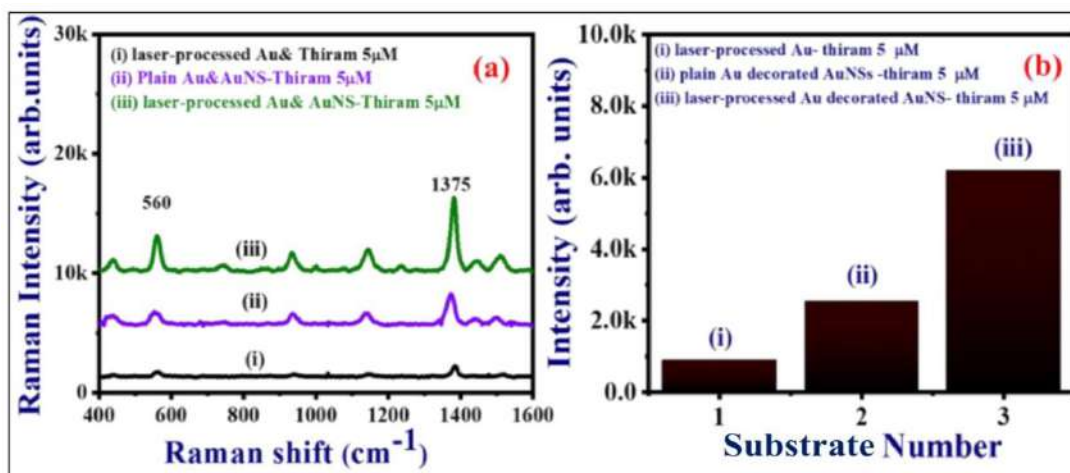


Fig 6. (a) Comparison of the SERS spectra of thiram $5 \mu\text{M}$ on (i) laser-processed Au without nanostars, (ii) plain Au with nanostars, (iii) laser-processed Au in the presence of nanostars, (b) SERS intensity of the prominent mode at 1375 cm^{-1} obtained from respective substrates.

The SERS spectra of Nile blue (NB) were recorded from laser-processed Au substrates decorated with Au nanostars at different concentrations (from $5 \mu\text{M}$ to 500 pM) and the data is illustrated in Fig 8(a). The Raman bands of NB were observed at 590 cm^{-1} and 663 cm^{-1} corresponding to the C-C-C and C-N-C deformations and in-plane C-C-C deformation, respectively. The NB peak intensities were enhanced

significantly with increasing concentration, and the detected lowest concentration was ~ 500 pM. Even at the 500 pM concentration, a few Raman modes of NB were still distinguishable, demonstrating the superior sensitivity of Au nanostars embedded laser-processed Au substrate. A logarithmic plot between the SERS signal intensity for the NB prominent mode at 590 cm^{-1} at different concentrations is shown in Fig 8(b). To evaluate the reproducibility of the SERS signal, SERS data of NB ($5\text{ }\mu\text{M}$) was collected at 25 random spots on the surface and the data is shown in Fig 8(c) as a 3D waterfall spectra. The RSD values for all observed Raman modes were found to be $<10\%$, as shown in the Fig 8(d).

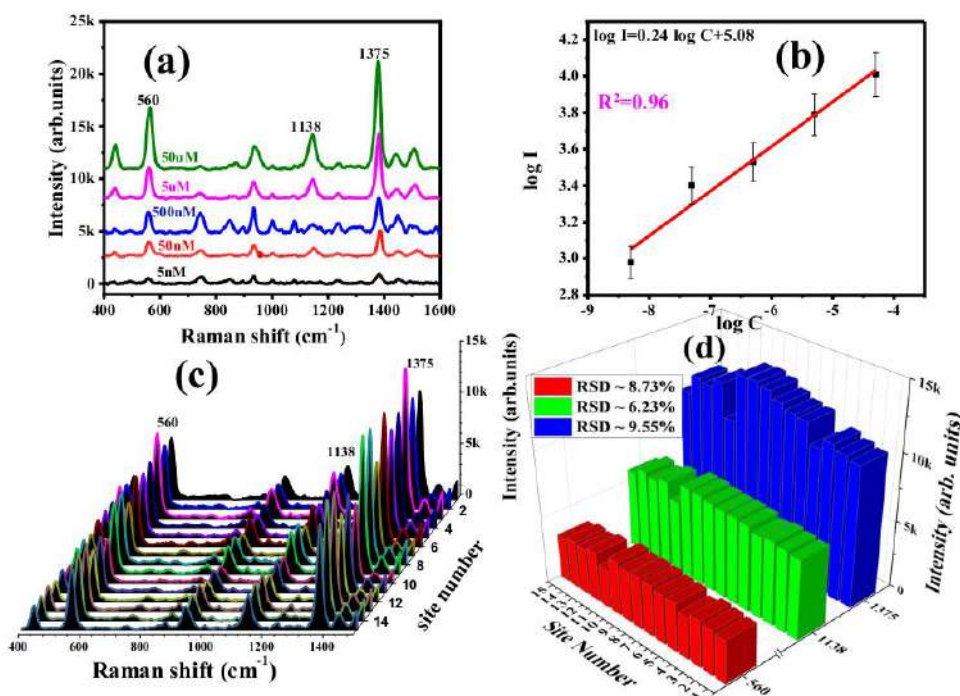


Fig 7. (a) Concentration-dependent SERS spectra of thiram recorded on nanostars embedded laser-processed Au (b) log plot between intensity and concentration (c) 3D waterfall spectra (d) SERS intensities of 560 cm^{-1} , 1138 cm^{-1} , and 1375 cm^{-1} achieved at randomly selected 15 spots.

Furthermore, the SERS efficiency of laser ablated Au NSs embedded with Au nanostars was examined with cytosine, a biomolecule one of the four building blocks/nucleotides of DNA, i.e., adenine, guanine, thymine, and cytosine [20]. Figure 9(a) represents the Raman spectra of cytosine, and the characteristic vibrational peaks of cytosine were indexed at $400, 547, 597, 789, 971, 1108, 1275, 1360, 1532,$ and 1654 cm^{-1} and are matched with the previous reports [21,22]. Figure 9(b) depicts the concentration-dependent SERS spectra of cytosine molecules from $300\text{ }\mu\text{M}$ to 30 nM ; the prominent peak at 781 cm^{-1} is highlighted and is assigned to ring breathing. The intensity of the significant peak decreases with decreasing concentration and is visible even at lower-level detection. The estimated EF (Enhancement factor) was $\sim 2.4 \times 10^5$ and the reproducibility of the substrate was investigated by recording the SERS signals of $300\text{ }\mu\text{M}$ cytosine from 20 random spots, the data are shown in Fig 9 (c). The peak intensity distributions of 781 cm^{-1} exhibited minor deviations with RSD value of $\sim 9\%$, and the bar graph is shown in Fig 9(d). Enhancement factor, defined as the increase in the Raman signal, of the three molecules (thiram, NB, and cytosine) achieved using Au NSs with nanostars was calculated using the relation $EF = [I_{\text{SERS}}/I_{\text{Raman}}][C_{\text{Raman}}/C_{\text{SERS}}]$, where, I_{SERS} : Intensity of the Raman signal obtained with the SERS substrate; I_{Raman} : Intensity of the Raman signal obtained

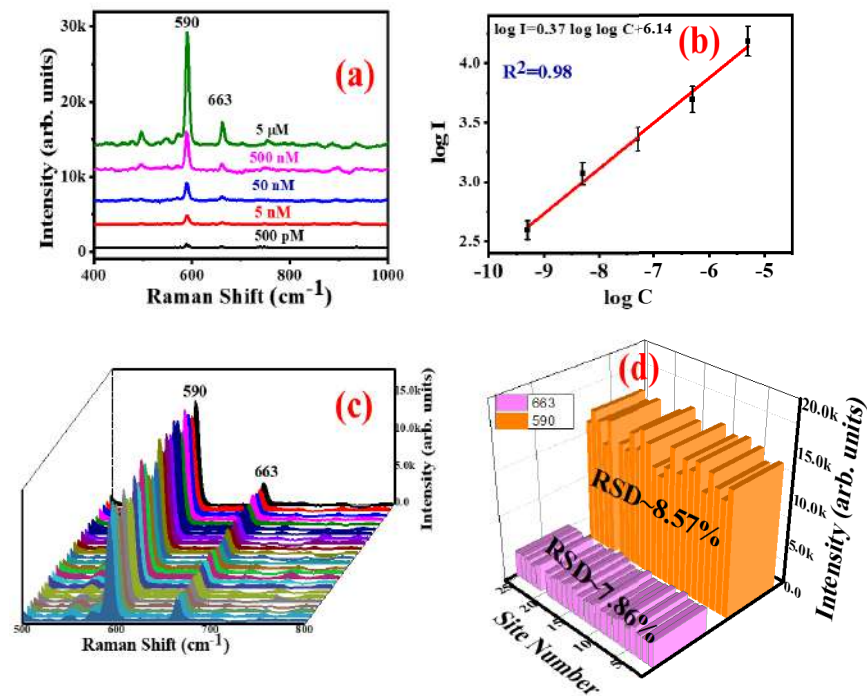


Fig 8. (a) SERS spectra of Nile blue (NB) with varying concentration from 500 pM to 5 μM on laser-processed Au decorated with Au nanostars (b) logarithmic plot of the 590 cm^{-1} Raman peak SERS intensity versus NB concentrations (c) 3D waterfall SERS spectra of NB (5 μM) at 25 spots (d) The 3D bar graph illustrates the RSD values estimated for the specific Raman modes at 663 cm^{-1} (depicted in pink color) and 590 cm^{-1} (shown in dark orange color).

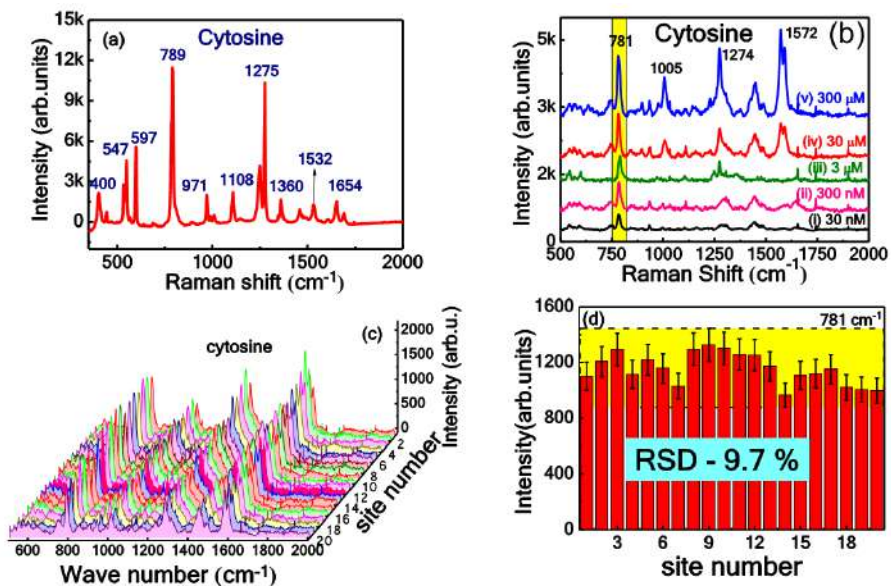


Fig 9. (a) Raman spectrum of cytosine (b) SERS spectra of cytosine 30 nM to 300 μM (c) 3D waterfall SERS spectra of cytosine (300 μM) at 20 random spots (d) Histogram of the calculated RSD of a particular Raman mode at 781 cm^{-1} .

without the SERS substrate (i.e., from the same analyte molecule in the absence of the substrate); C_{Raman} : Concentration of the analyte molecule used for obtaining the Raman signal without the SERS substrate; C_{SERS} : Concentration of the analyte molecule used for obtaining the Raman signal with the SERS substrate [23]. The obtained EFs were $\sim 10^5$ for all the investigated molecules.

4 Conclusions

In summary, the ps-laser-fabricated Ag NPs and Au NSs were successfully used as efficient SERS substrates. The stability and the size of Ag NPs can be modified by changing the surrounding medium. Further, Au nanostars embedded in plain and laser-processed Au substrates were used as SERS active platforms for detecting thiram, Nile blue and cytosine. The as-fabricated Au nanostars embedded laser processed Au exhibited higher enhancements and lower detection limits of 5 nM in the case of thiram, 500 pM in the case of NB, and 30 nM for cytosine molecule with enhancement factors of $\sim 10^5$. The present study provides a possible way to improve the detection limits of different analyte molecules (e.g., pesticides, dyes) with a combination of nanostars and laser patterned nanostructured surfaces.

Acknowledgments

Venugopal Rao Soma acknowledges the DRDO (ERIP/ER/1501138/M/01/319/D(R&D)) for financial support through ARCHEM, University of Hyderabad (UoH). VRS and MSSB thank the UoH for support through a project under the aegis of Institute of Eminence (# UOH/IOE/RC1/RC1-20-016). We thank the Director, ACRHEM (Dr V Kameswara Rao) for his support and encouragement.

References

1. Li J, Lin H, Zhang X, Li M, Seed shape-controlled, facet-selective growth of superspiky gold nanocrystals for biosensing applications, *J Mater Chem C*, 9(2021)8694; doi.org/10.1039/D1TC02083H.
2. Terry L R, Sanders S, Potoff R H, Krueel J W, Jain M, Guo H, Applications of surface-enhanced Raman spectroscopy in environmental detection, *Anal Sci Adv*, 3(2022)113–145.
3. Nehra K, Pandian S K, Bharati M S S, Soma V R, Enhanced catalytic and SERS performance of shape/size controlled anisotropic gold nanostructures, *New J Chem*, 43(2019)3835–3847.
4. Guerrero-Martínez A, Barbosa S, Pastoriza-Santos I, Liz-Marzán L M, Nanostars shine bright for you: colloidal synthesis, properties and applications of branched metallic nanoparticles, *Curr Opin Colloid Interface Sci*, 16 (2011)118–127.
5. Ma J, Liu X, Wang R, Zhang J, Jiang P, Wang Y, Tu G, Bimetallic core-shell nanostars with tunable surface plasmon resonance for surface-enhanced Raman scattering, *ACS Appl Nano Mater*, 3(2020)10885–10894.
6. Kumar P S, Pastoriza-Santos I, Rodríguez-González B, De Abajo F J G, Liz-Marzán L M, High-yield synthesis and optical response of gold nanostars, *Nanotechnology*, 19(2007)015606; doi. 10.1088/0957-4484/19/01/015606.
7. Nehra K, Pandian S K, Byram C, Moram S S B, Soma V R, Quantitative analysis of catalysis and SERS performance in hollow and star-shaped Au nanostructures, *J Phys Chem*, 123(2019)16210–16222.
8. Zhu J, Liu M-J, Li J-J, Li X, Zhao J-W, Multi-branched gold nanostars with fractal structure for SERS detection of the pesticide thiram, *Spectrochim Acta*, A189(2018)586–593.
9. Moram S S B, Byram C, Soma V R Gold-nanoparticle-and nanostar-loaded paper-based SERS substrates for sensing nanogram-level Picric acid with a portable Raman spectrometer, *Bull Mater Sci*, 43(2020)53; doi.org/10.1007/s12034-019-2017-8.
10. Zeng H, Du X W, Singh S C, Kulinich S A, Yang S, He J, Cai W, Nanomaterials via Laser Ablation/Irradiation in Liquid: A Review, *Adv Funct Mater*, 22(2012)1333–1353.
11. Fazio E, Gökce B, De Giacomo A, Meneghetti M, Compagnini G, Tommasini M, Waag F, Lucotti A, Zanchi C G, Ossi P M, Nanoparticles Engineering by Pulsed Laser Ablation in Liquids: Concepts and Applications, *Nanomaterials*, 10(2020)2317; doi.org/10.3390/nano10112317.

12. Barcikowski S, Hahn A, Kabashin A V, Chichkov B N, Properties of nanoparticles generated during femtosecond laser machining in air and water, *Appl Phys A*, 87(2007)47–55.
13. Rao S V, Podagatlapalli G K, Hamad S, Ultrafast laser ablation in liquids for nanomaterials and applications, *J Nanosci Nanotechnol*, 14(2014)1364–1388.
14. Semerok A, Chaléard C, Detalle V, Lacour J L, Mauchien P, Meynadier P, Nouvellon C, Sallé B, Palianov P, Perdrix M, Petite G, Experimental investigations of laser ablation efficiency of pure metals with femto, pico and nanosecond pulses, *Appl Surf Sci*, 138–139(1999)311–314.
15. Byram C, Moram S S B, Soma V R, SERS based detection of multiple analytes from dye/explosive mixtures using picosecond laser fabricated gold nanoparticles and nanostructures, *Analyst*, 144(2019)2327–2336.
16. Šišková K, Vlčková B, Turpin P Y, Fayet C, Ion-specific effects on laser ablation of silver in aqueous electrolyte solutions, *J Phys Chem C*, 112 (2008)4435–4443.
17. Osorio M F, Salazar A, Prieto F, Boulanger P, Figueroa P, Three-dimensional digitization of highly reflective and transparent objects using multi-wavelength range sensing, *Machine Vision and Applications*, 23 (2012)761–772.
18. Rathod J, Byram C, Kanaka R K, Bharati M S S, Banerjee D, Akkanaboina M, Soma V R, Hybrid surface-enhanced Raman scattering substrates for the trace detection of ammonium nitrate, thiram, and Nile blue, *ACS Omega*, 18(2022)15969–15981.
19. Moram S S B, Shaik A K, Byram C, Hamad S, Soma V R, Instantaneous trace detection of nitro-explosives and mixtures with nanotextured silicon decorated with Ag–Au alloy nanoparticles using the SERS technique, *Anal Chim Acta*, 1101(2019)157–168.
20. Madzharova F, Heiner Z, Gühlke M, Kneipp J, Surface-enhanced hyper-Raman spectra of adenine, guanine, cytosine, thymine, and uracil, *J Phys Chem C*, 120(2016)15415–15423.
21. Liu S, Zheng G, Li J, Raman spectral study of metal–cytosine complexes: A density functional theoretical (DFT) approach, *Spectrochim Acta*, A79(2011)1739–1746.
22. Vendamani V S, Beeram R, Neethish M M, Rao S V S N, Rao S V, Wafer-scale silver nanodendrites with homogeneous distribution of gold nanoparticles for biomolecules detection, *iScience*, 25(2022)104849; doi.org/10.1016/j.isci.2022.104849.
23. Ru E C L, Blackie E, Meyer M, Etchegoin P G, Surface enhanced Raman scattering enhancement factors: a comprehensive study, *J Phys Chem C*, 111(2007)13794–13803.

[Received: 05.01.2022; revised recd: 26.02.2023; accepted: 28.02.2023]